

## Reversible low-field magnetocaloric effect in Ni-Mn-In-based Heusler alloys

Jun Liu <sup>1,2,\*</sup> Xinmin You,<sup>1</sup> Bowei Huang,<sup>1</sup> Ivan Batashev,<sup>1</sup> Michael Maschek,<sup>1</sup> Yuanyuan Gong,<sup>2</sup> Xuefei Miao,<sup>2</sup> Feng Xu,<sup>2,\*</sup> Niels van Dijk,<sup>1</sup> and Ekkes Brück<sup>1</sup>

<sup>1</sup>*Fundamental Aspects of Materials and Energy (FAME), Delft University of Technology, Mekelweg 15, 2629 JB Delft, The Netherlands*

<sup>2</sup>*MIT Key Laboratory of Advanced Metallic and Intermetallic Materials Technology, School of Materials Science and Engineering, Nanjing University of Science and Technology, Nanjing 210094, People's Republic of China*



(Received 24 May 2019; published 14 August 2019)

Ni-Mn- $X$  ( $X = \text{In, Sn, and Sb}$ ) based Heusler alloys show a strong potential for magnetic refrigeration owing to their large magnetocaloric effect (MCE) associated with first-order magnetostructural transition. However, the irreversibility of the MCE under low field change of 0–1 T directly hinders its application as an efficient magnetic coolant. In this work, we systematically investigate thermal and magnetic properties, crystalline structure and magnetocaloric performance in  $\text{Ni}_{51-x}\text{Mn}_{33.4}\text{In}_{15.6}\text{V}_x$  alloys. With the introduction of V, a stable magnetostructural transition near room temperature is observed between martensite and austenite. An extremely small hysteresis of 2.3 K is achieved for the composition  $x = 0.3$ . Due to this optimization, the magnetic-field induced structural transition is partially reversible under 0–1 T cycles, resulting in a reversible MCE. Both magnetic and calorimetric measurements consistently show that the largest value for the reversible magnetic entropy change can reach about  $5.1 \text{ J kg}^{-1} \text{ K}^{-1}$  in a field change of 0–1 T. A considerable and reversible adiabatic temperature change of  $-1.2 \text{ K}$  by the direct measurement is also observed under a field change of 0–1.1 T. Furthermore, the origin of this small hysteresis is discussed. Based on the lattice parameters, the transformation stretch tensor is calculated, which indicates an improved geometric compatibility between the two phases. Our work greatly improves the MCE performance of Ni-Mn- $X$ -based alloys and make them suitable as realistic magnetic refrigeration materials.

DOI: [10.1103/PhysRevMaterials.3.084409](https://doi.org/10.1103/PhysRevMaterials.3.084409)

### I. INTRODUCTION

The magnetocaloric effect (MCE), the thermal response of materials exposed to a magnetic field, is an important magneto-responsive phenomenon [1,2]. On the basis of this effect, the most developed solid-state refrigeration, magnetic refrigeration (MR), can be realized with proper magnetic cooling cycles [3]. As a green and efficient energy conversion technology, MR at ambient temperature has attracted a lot of attention since the discovery of the giant MCE in the  $\text{Gd}_5(\text{Si}_2\text{Ge}_2)$  system, which is derived from the first-order magnetic phase transition [4]. Both experimental approaches and theoretical calculations have confirmed that a giant MCE can be expected in materials where the magnetism and the crystalline structure strongly couple [5,6]. Nowadays, a number of promising candidate materials for room-temperature MR have been proposed, including (Mn,Fe)(P,X)-based compounds ( $X = \text{As, Ge, Si}$ ) [7–9],  $\text{La}(\text{Fe, Si})_{13}$ -based materials [10,11], Ni-Mn- $X$  based Heusler alloys ( $X = \text{In, Sn, Sb}$ ) [12–16], and the  $\text{Mn}(\text{Co,Ni})(\text{Ge,Si})$  system [17–19].

Ni-Mn- $X$  based Heusler alloys, in which the lattice structure consists of four interpenetrating *fcc* sublattices, exhibit a magnetostructural transition (MST) from the ferromagnetic cubic austenite to the weakly magnetic martensite with a lower symmetry [12–16,20–22]. Due to the coupling of ferromagnetism and ferroelasticity, multifunctional effects, such

as caloric effects, magnetostrain effect, and magnetoresistance can be triggered under external stress or magnetic field [12–16,23–27]. From the viewpoint of the MCE, the entropy changes of the lattice and the magnetism mainly contribute to the total entropy change ( $\Delta S_t$ ) during the martensitic transition [28,29]. The lattice part is stronger than the competing magnetic part, which leads to the so-called inverse MCE [12,15]. Therefore, the material cools when magnetized adiabatically and the entropy increases under isothermal conditions. The remarkable magnetocaloric performance, together with the reasonably good mechanical properties originating from the strong *p-d* covalent bonding [30], makes the system an outstanding magnetic refrigerant.

However, Ni-Mn- $X$ -based materials are currently seldom used in lab-scale MR prototypes. The main problem with these materials is that the inherent hysteresis phenomenon linked to the MST causes functional fatigue of the MCE during cycling. Recently, some studies have focused on the improvement of the reversibility for the magnetic-field-induced MST and the accompanying MCE in Ni-(Co)-Mn-In and Ni-(Co)-Mn-Sn systems [31–34]. Unfortunately, the studied compositions only show a giant reversible magnetic entropy change or adiabatic temperature change ( $\Delta S_m$  or  $\Delta T_{ad}$ ) under a 5-T field variation or a moderate effect under a 2-T field variation. Current demonstrators operate with an active magnetic refrigeration cycle using Nd-Fe-B permanent magnets as the field source [35]. As the most expensive part, the rare-earth-based field source should be scaled down as much as possible, which effectively limits the magnetic field in

\*Corresponding authors: J.Liu-7@tudelft.nl; xufeng@njust.edu.cn

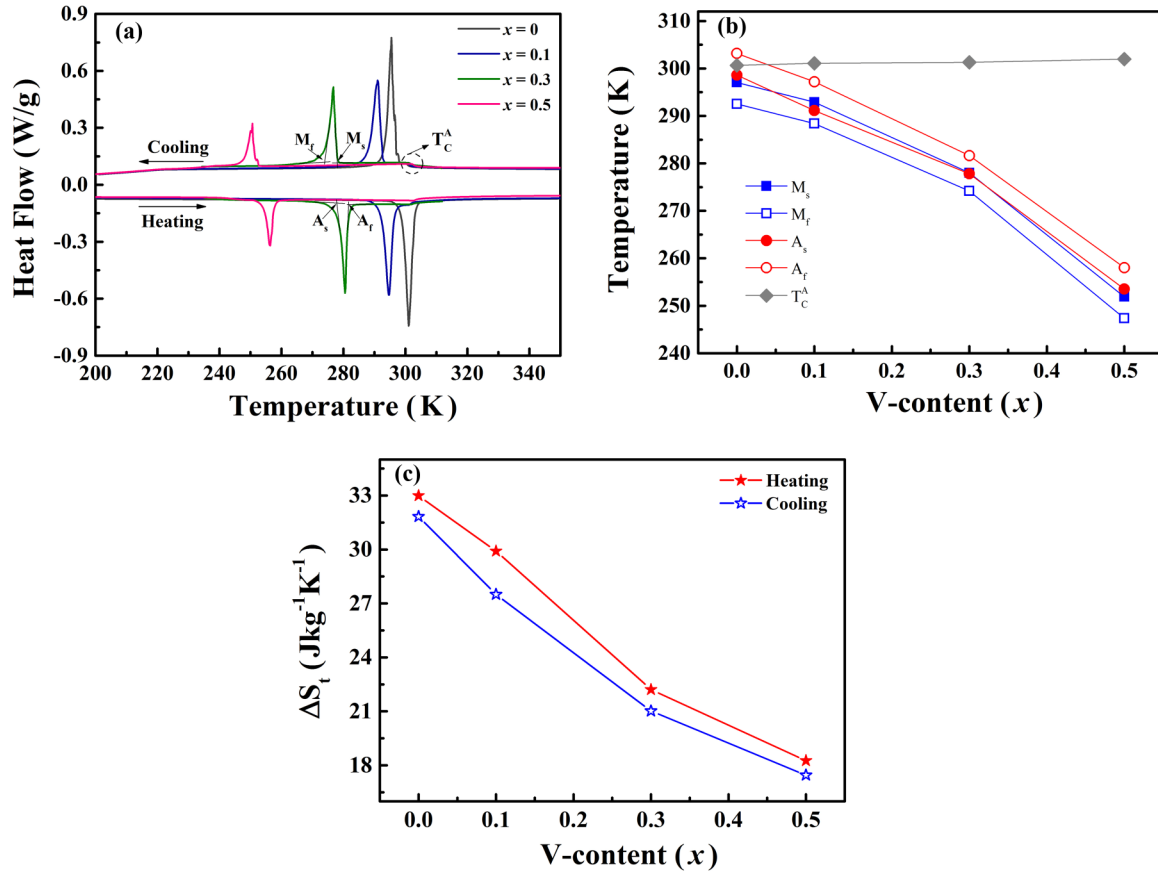


FIG. 1. (a) DSC curves during heating and cooling for  $\text{Ni}_{51-x}\text{Mn}_{33.4}\text{In}_{15.6}\text{V}_x$ . (b) Characteristic temperatures and (c) total entropy change during the structural transition extracted from the DSC curves as a function of the V content.

the range of 1 T [35–37]. Under this low field variation, it appears that the MST cannot be induced completely. In addition, this partial transition would significantly degrade in the subsequent magnetic cycles. We should therefore aim to achieve a sizeable and reversible MCE in Ni-Mn-X system under a modest field change of 0–1 T.

In this work, we have investigated the MCE and its reversibility in  $\text{Ni}_{51-x}\text{Mn}_{33.4}\text{In}_{15.6}\text{V}_x$  system. By introducing a small amount of V into the base composition  $\text{Ni}_{51}\text{Mn}_{33.4}\text{In}_{15.6}$ , the structural transition temperature ( $T_t$ ) is tuned. Surprisingly, the associated thermal hysteresis can be reduced to a very small value of 2.3 K for the sample with  $x = 0.3$ . Due to this improvement, a reversible MCE in low field can be obtained in both magnetic and calorimetric measurements. Furthermore, the origin of this small hysteresis is discussed from the viewpoint of the kinematic compatibility.

## II. EXPERIMENTAL

Polycrystalline samples with a nominal composition of  $\text{Ni}_{51-x}\text{Mn}_{33.4}\text{In}_{15.6}\text{V}_x$  ( $x = 0, 0.1, 0.3, 0.5, 1.0$ ) were prepared by arc melting high-purity ( $\geq 99.9\%$ ) raw materials under Ar atmosphere for four times. The as-cast ingots sealed in quartz tubes in Ar atmosphere were annealed at 1173 K for 24 h in and then quenched into cold water. The calorimetric measurements were carried out in a commercial differential scanning calorimeter (DSC, TA Instrument Q2000) with

heating/cooling rate of 10 K/min.  $\Delta S_m$  and  $\Delta T_{ad}$  were calculated based on the specific heat measurements under different magnetic fields by a homebuilt Peltier cell-based DSC [38]. The direct  $\Delta T_{ad}$  measurement using a temperature sweeping mode was performed on a homemade device with a maximum field of 1.1 T, described in detail in Ref. [8]. The magnetic properties were characterized by a superconducting quantum interference device (SQUID, Quantum Design MPMS 5XL) with the reciprocating sample option. To further evaluate  $\Delta S_m$  based on the Maxwell relation, the isofield temperature dependence of magnetization ( $M$ - $T$ ) curves were recorded at a rate of 1 K/min with a field increment of 0.2 T. The temperature dependence of the powder x-ray diffraction (XRD, PANalytical X'Pert PRO) were collected with an Anton Paar TTK450 low-temperature chamber. The structure refinement of the XRD patterns was performed using Fullprof's implementation of the Rietveld refinement method [39].

## III. RESULTS AND DISCUSSION

Figure 1(a) shows the DSC curves for the  $\text{Ni}_{51-x}\text{Mn}_{33.4}\text{In}_{15.6}\text{V}_x$  ( $x = 0, 0.1, 0.3$  and  $0.5$ ) alloys. The temperature marked as  $M_s$ ,  $M_f$ ,  $A_s$ , and  $A_f$  denote the start and finish points of martensitic transition and austenitic transition, respectively. All the studied samples exhibit large endothermic/exothermic peaks during the heating/cooling processes. The obvious thermal hysteresis ( $\Delta T_{\text{hys}}$ ) indicates

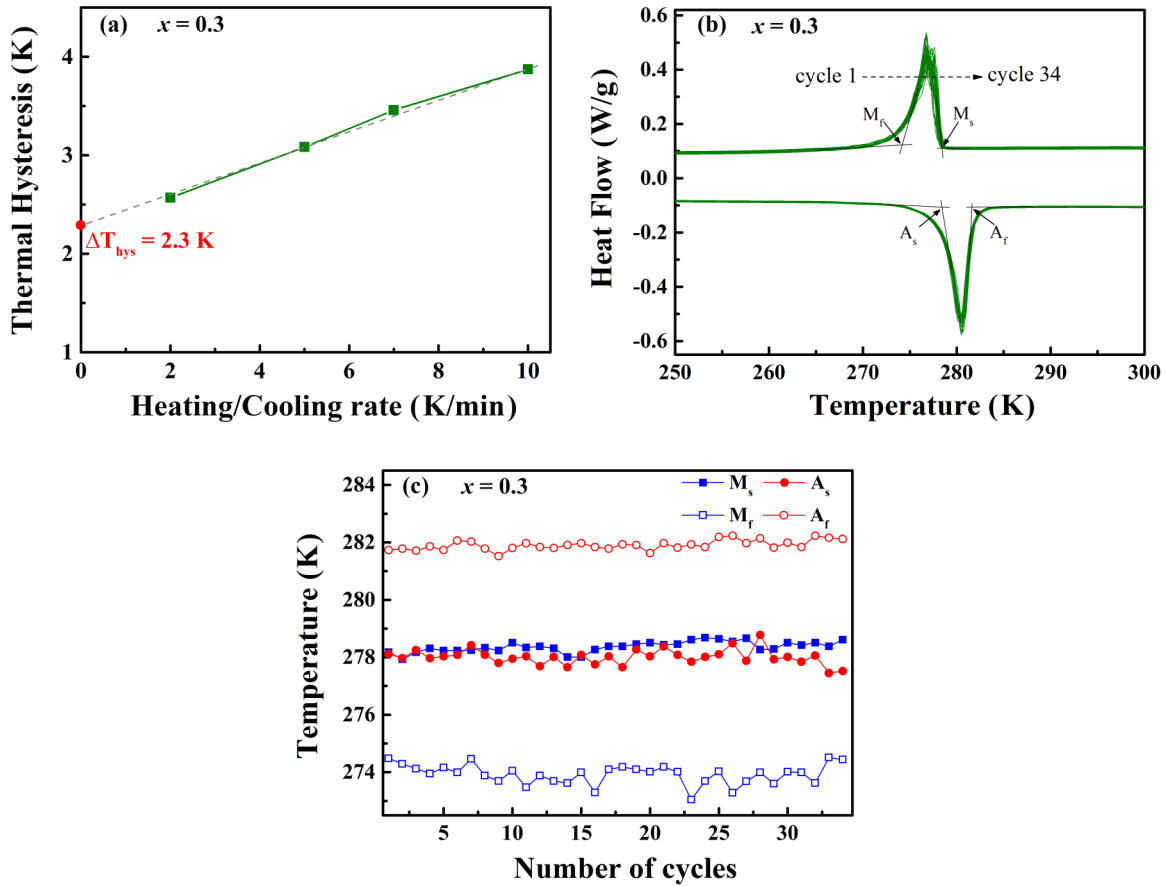


FIG. 2. (a) Thermal hysteresis obtained from DSC curves for  $\text{Ni}_{51-x}\text{Mn}_{33.4}\text{In}_{15.6}\text{V}_x$  measured at different sweep rates. (b) DSC curves and (c) characteristic transformation temperatures under 34 thermal cycles for sample with  $x = 0.3$ .

the first-order nature of the structural transition. The relatively small kinks above the structural transition temperature [defined as  $T_t = (M_s + M_f)/2$  or  $(A_s + A_f)/2$ ] correspond to the Curie temperature of the austenite ( $T_C^A$ ). The characteristic temperatures as a function of the variation in V content are plotted in Fig. 1(b). Since the martensitic transition is sensitive to the valence electron concentration in Ni-Mn-X-based alloys [22], the introduction of V with less valence electrons than Ni rapidly reduces  $T_t$ . While  $T_C^A$ , which is primarily determined by the strong nearest-neighbor exchange interactions for Ni-Mn and Mn-Mn pairs [40], is stable due to the small amount of V doping. In this case, the distance between  $T_C^A$  and  $T_t$  increases with increasing V content, which results in the larger magnetization difference of austenite and martensite. Therefore, the magnetic part in the MST and the associated magnetostructural coupling is strengthened [41]. Consequently, due to the competition between the structural and the magnetic contributions to the  $\Delta S_t$ , the endothermic/exothermic peaks weaken and  $|\Delta S_t|$  during the transition decreases [shown in Fig. 1(c)].  $\Delta S_t$  is calculated by

$$\Delta S_t = \int_{A_s}^{A_f} (\dot{Q} - \dot{Q}_{\text{baseline}}) \left( \frac{\partial T}{\partial t} \right)^{-1} dT, \quad (1)$$

where  $\dot{Q}$  is the heat flow and  $\dot{Q}_{\text{baseline}}$  denotes the baseline of  $\dot{Q}$ , which is obtained by adopting a smooth line across the transition.

As inferred before, a low  $\Delta T_{\text{hys}}$  is beneficial to the reversibility of MCE. Here, we find that the hysteresis width (defined as  $\Delta T_{\text{hys}} = (A_s + A_f - M_s - M_f)/2$ ) decreases to a low value by increasing the V content to 0.3. To eliminate the thermal lag problems during the measurement, a precise value of  $\Delta T_{\text{hys}}$  at steady state is determined by extrapolating the results for different sweep rates toward a zero-sweep rate, as shown in Fig. 2(a). Consequently, a  $\Delta T_{\text{hys}}$  of 2.3 K is achieved for the sample with  $x = 0.3$ , which is extremely small in comparison with other Ni-Mn-X-based Heusler alloys [12–16,20–29,31–34]. Due to the optimization of the hysteresis, the sample can resist the large migration of  $T_t$  under thermal cycles. As presented in Figs. 2(b) and 2(c), the martensitic transitions almost overlap with each other and the characteristic transition temperatures fluctuate only in a narrow range over 34 cycles.

Apart from small  $\Delta T_{\text{hys}}$ , the establishment of a magnetostructural coupling is the premise of large reversible MCE. As revealed in the  $M$ - $T$  curves in a field of 0.01 T in Fig. 3(a),  $T_t$  is reduced to a value below than  $T_C^A$  with increasing V content. Thus, an MST with sharp magnetization change ( $\Delta M$ ) is observed. In the martensitic state, a magnetic disorder-order transition is found. Additionally, zero-field-cooling (ZFC) and field-cooling (FC) curves exhibit an obvious separation originated from the coexistence of ferromagnetic and antiferromagnetic configurations [42]. The obtained hysteresis widths obtained from  $M$ - $T$  curves in Figs. 3(a) and 3(b) are consistent

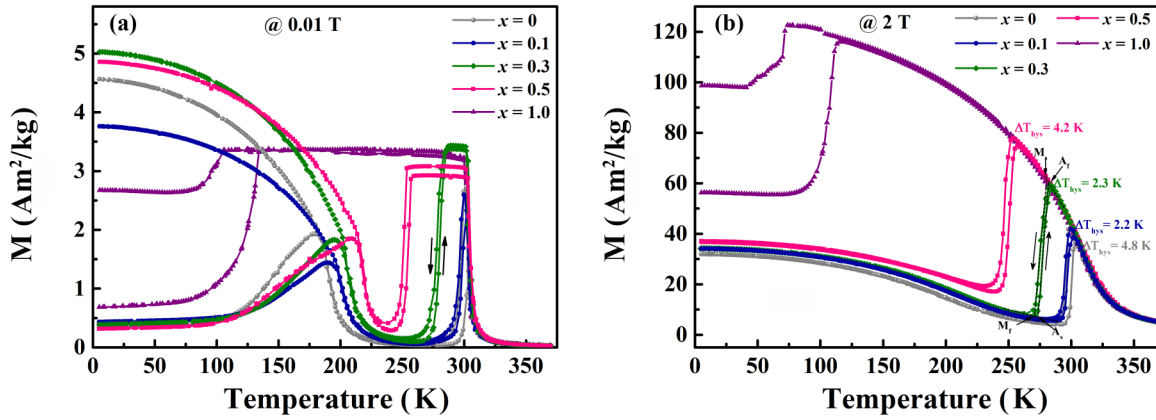


FIG. 3. ZFC and FC  $M$ - $T$  curves for an applied field of (a) 0.01 T and (b) 2 T of  $\text{Ni}_{51-x}\text{Mn}_{33.4}\text{In}_{15.6}\text{V}_x$  alloys. The characteristic temperatures- $M_s$ ,  $M_f$ ,  $A_s$ , and  $A_f$  are indicated and  $\Delta T_{\text{hys}}$  are listed.

with those from DSC results. It should be noted that samples with  $x = 0.1$  and  $x = 0.3$  both possess a very small  $\Delta T_{\text{hys}}$  of 2.2 and 2.3 K, respectively. Sample with  $x = 0.3$  with a relatively larger  $\Delta M$  and lower  $\Delta S_f$ , shows a stronger effect of the magnetostructural coupling, which is more favorable for the reversibility of the MCE [43]. Specifically, the sensitivity of  $T_i$  to the magnetic field is about  $-2$  K/T in sample with  $x = 0.3$  as estimated from the  $M$ - $T$  curves or by applying the Clausius-Clapeyron relation ( $\Delta T_i / \Delta \mu_0 H = -\Delta M / \Delta S_f$ ).

When a field of 1 T is applied, the shift in  $T_i$  is comparable to the  $\Delta T_{\text{hys}}$  in sample with  $x = 0.3$ , which indicates that a partially reversible field-induced MST could be achieved [33,44]. Figure 4 shows the isothermal  $M$ - $B$  curves under two successive 0–1 T cycles measured by the so-called loop-method [45]. As the magnetic field is prone to stabilize the FM state, the field-induced MST accompanied by a large magnetic hysteresis occurs with the first application of 1 T. When the magnetic field decreases, as a result of  $\Delta T_{\text{hys}}$ , the induced austenite cannot transform back completely and residual austenite is preserved. As shown in Fig. 4, the “trapped” residual austenite results in an increase of magnetization in

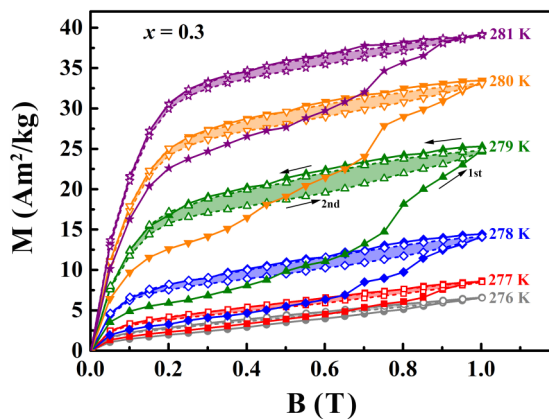


FIG. 4. Isothermal magnetization curves as a function of the applied magnetic field around  $T_i$  in the field range of 0–1 T under two magnetic cycles for the sample with  $x = 0.3$ . The measurements are performed in the heating process.

the subsequent cycle due to its ferromagnetism. However, profiting from the small value of  $\Delta T_{\text{hys}}$ , part of the sample can transform back and forth, as indicated by the obvious magnetic hysteresis during the second cycle. As a result, this “untrapped” part would contribute to the reversible MCE even under a field change of 0–1 T.

The magnetic entropy change  $\Delta S_m$ , the crucial parameter to evaluate the MCE, is calculated by the Maxwell relation:

$$\Delta S_m = \int_0^B \left( \frac{\partial M}{\partial T} \right)_B dB. \quad (2)$$

As shown in Fig. 5(a), the sample with  $x = 0.3$  exhibits a positive  $\Delta S_m$  in the MST region, indicating an inverse MCE. In the heating process, the maximum value of  $\Delta S_m$  reaches  $7.2 \text{ J kg}^{-1} \text{ K}^{-1}$  at 279 K for a low field change of 0–1 T. Evidently, the entropy change cannot reach the saturation value  $\Delta S_f$  under this low field variation, which manifests that only a partial MST occurs. It is reported that the cyclic  $\Delta S_m$  can be estimated by the area where the cooling and heating branches of  $\Delta S_m$  versus temperature curves overlap (yellow area in Fig. 5) [46,47]. The largest reversible value is about  $5.1 \text{ J kg}^{-1} \text{ K}^{-1}$  under 0–1 T field variation, which is higher than that of the archetypal magnetocaloric Gd [3,4]. Moreover, we show the reversible  $\Delta S_m$  under a field change of 0–5 T in the inset of Fig. 5(a) (the details are shown in the Supplementary Material [48]). Because a larger fraction of the MST is involved to contribute to the inverse MCE in a higher field, a large reversible  $\Delta S_m$  of  $18.9 \text{ J kg}^{-1} \text{ K}^{-1}$  is achieved in a field change of 5 T at 274 K, which is comparable with the highest value reported in the Ni-Mn-X-based alloys [49]. Notably, a broad and reversible conventional MCE is also present in the higher temperature range that originates from the second-order magnetic transition of austenite. In addition, the entropy change can be also determined by the heat capacity curves at different magnetic fields according to the following equation:

$$\Delta S_m = \int_{T_0}^T \frac{1}{T} [C_p(T, B) - C_p(T, 0)] dT, \quad (3)$$

where  $T_0$  is the start temperature in the DSC experiment (242 K in this case). As shown in the inset of Fig. 5(b), the

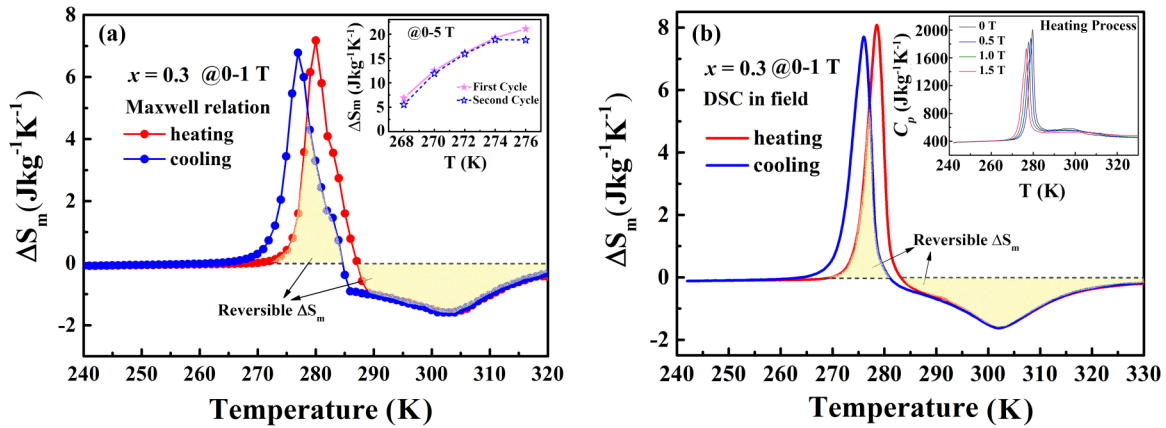


FIG. 5. Magnetic entropy change ( $\Delta S_m$ ) as a function of temperature for the heating and cooling processes determined by (a) the Maxwell relation and (b) the specific heat in field (shown in the inset) for sample with  $x = 0.3$ . The yellow area represents the reversible part of the entropy change. The inset of Fig. 3(a) shows  $\Delta S_m$  under two magnetic cycles with a field change of 0–5 T.

specific heat curve shifts to a lower temperature range with the application of magnetic field. The  $\Delta S_m$  as a function of temperature is consistent with that from magnetic measurements, which guarantees the validity of the obtained entropy change.

In order to further confirm the high degree of reversibility for  $\Delta S_m$ , a cyclic magnetic field was applied under isothermal condition. The results are shown in Fig. 6(a). Before each measurement, the sample was first cooled down to 240 K, and then heats up to the target temperature slowly. At 278.5 K, sample with  $x = 0.3$  exhibits an obvious endothermic peak when a field of 1 T is applied and releases heat after the field is removed, which is a direct signature of the inverse MCE. In the second field cycle, the exo-/endothermic peaks drop while the value keeps stable during the subsequent cycles, which indicates the presence of a reversible MCE. The so-obtained reversible entropy change is about  $4.6 \text{ J kg}^{-1} \text{ K}^{-1}$ . In contrast, the sample with  $x = 0.3$  shows a typical conventional MCE at 300 K, where it releases (absorbs) heat by applying (removing) magnetic field, as presented in the inset of Fig. 6(b).

Apart from  $\Delta S_m$ , adiabatic temperature change  $\Delta T_{ad}$  is also estimated from an indirect calorimetric method (DSC in

field), which is considered as the most straightforward assessment of the MCE. As shown in Fig. 7(a), a maximum value of  $-1.8 \text{ K}$  is obtained by applying a field of 1 T. To further investigate the reversibility of  $\Delta T_{ad}$ , the direct measurement of  $\Delta T_{ad}$  is performed using temperature sweeping mode. The raw data in Fig. 7(b) show that the temperature decreases (increases) with the application (removal) of magnetic field of 1.1 T, which indicates a highly reversible inverse MCE. Therefore, the reversible  $\Delta T_{ad}$  as a function of temperature is extracted as shown in Fig. 7(c). The largest reversible  $\Delta T_{ad}$  is about  $-1.2 \text{ K}$  for  $\Delta B = 1.1 \text{ T}$  around MST. This relatively large value is ascribed to the small hysteresis and the strong magnetostructural coupling.

In shape memory alloys (SMAs), it is widely believed that  $\Delta T_{hys}$  is derived from the energy barrier for nucleation of the new phase caused by the stressed transition layer during the thermoelastic martensitic transition [50–52]. Due to the existence of such a layer, the functional properties, as well as the structural integrity, are prone to fatigue during cycling of the external field [51,53]. A recent crystallographic theory of martensite indicates that the stressed layer can be eliminated through improving the geometric compatibility between the two phases, and thereby significantly reducing  $\Delta T_{hys}$  [50–54].

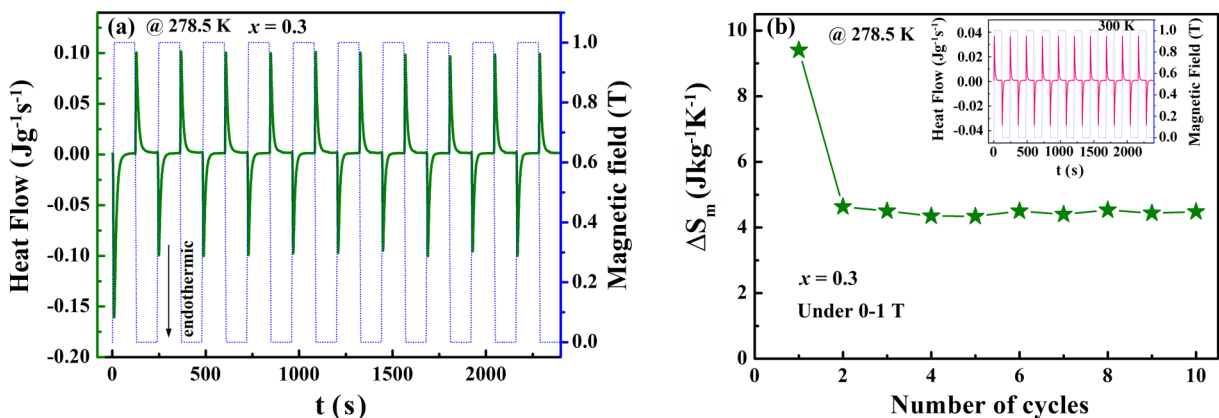


FIG. 6. (a) Calorimetric curves (solid line) obtained under isothermal conditions with a cyclic application/removal of the magnetic field (blue dash line) at 278.5 K. (b)  $\Delta S_m$  in 10 field cycles of 0–1 T. The inset is the calorimetric curves under cyclic fields at 300 K.

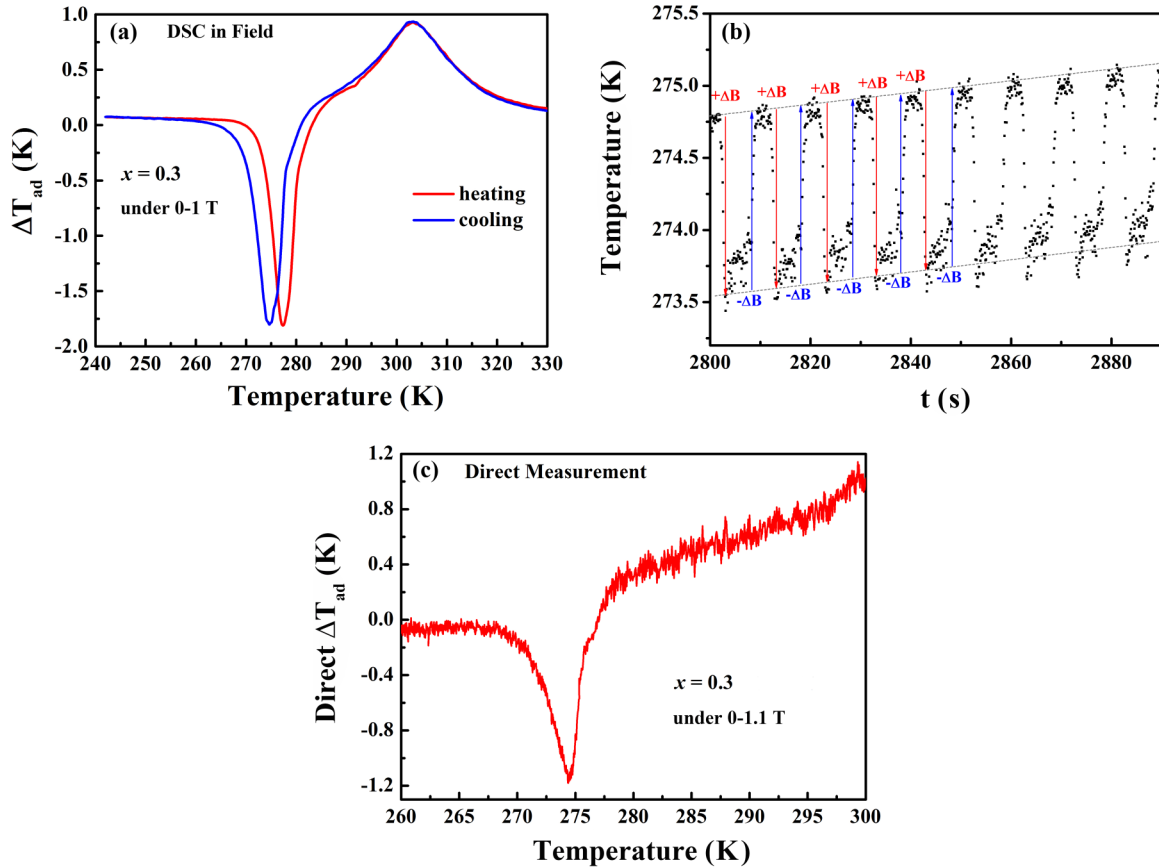


FIG. 7. (a) Temperature dependence of  $\Delta T_{ad}$  from DSC measurements for  $\Delta B = 1$  T. (b) Temperature versus time during direct  $\Delta T_{ad}$  measurements in sweep mode for  $\Delta B = 1.1$  T. (c)  $\Delta T_{ad}$  versus temperature evolution during the temperature sweep.

In this theory, the compatibility is satisfied when the middle eigenvalue  $\lambda_2$  of the transformation stretch tensor  $\mathbf{U}$  is close to one [50–54].

For magnetic SMAs, the strong correlation between the hysteresis width and  $\lambda_2$  has been widely reported in Ni-Mn-X-based Heusler alloys [15,16,27,33,49,55,56]. The determination of  $\lambda_2$  relies on the crystalline structures of austenite and martensite and their lattice parameters [57]. Thus, temperature-dependent powder XRD is carried out for the sample with  $x = 0.3$ , as shown in Fig. 8(a). It is clear that the dominant (110) reflection of parent phase splits into four reflections, which is ascribed to the Bain distortion during the martensitic transition [58]. In the refinement we identified that the martensite and the parent austenite have a modulated monoclinic structure and a  $L2_1$ -type cubic structure, respectively. The trace of austenitic patterns at 250 K and martensitic patterns at 340 K can be attributed to a residual stress generated upon grinding the ingot into powder [54,59]. In the analysis the phase transition temperature should be chosen such that the two phases coexist. At 270 K, the lattice parameters are  $a_M = 4.3358(4)$  Å,  $b_M = 5.6827(7)$  Å,  $c_M = 4.3212(4)$  Å,  $\beta_M = 92.11(5)^\circ$  for martensite and  $a_A = 5.9968(3)$  Å for austenite. Theoretically, there are 12 stretch tensors in the cubic-monoclinic-type transition, which correspond to 12 unique martensitic variants within the cubic basis [57]. These tensors have the same eigenvalues and the components are related by symmetry. One of these tensors is

shown below:

$$\mathbf{U} = \begin{pmatrix} 1.0223(3) & 0 & -0.0188(4) \\ 0 & 0.9476(1) & 0 \\ -0.0188(4) & 0 & 1.0189(2) \end{pmatrix}.$$

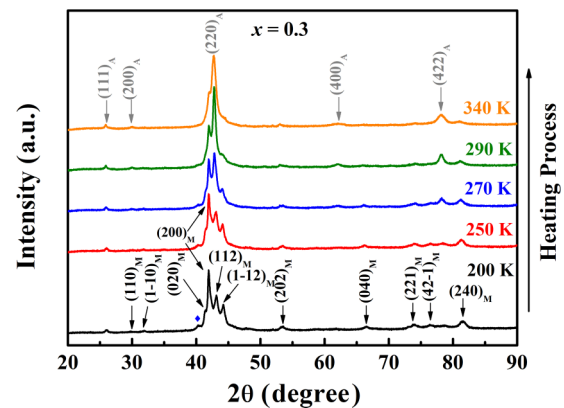


FIG. 8. Temperature dependence of the XRD patterns for the sample with  $x = 0.3$  for increasing the temperatures. The crystal indices of austenite and martensite are indicated. The minor peak (blue diamond) corresponds to the satellite reflections generated by a structural modulation.

From this tensor the eigenvalues are calculated:  $\lambda_1 = 0.9476(2)$ ,  $\lambda_2 = 1.0017(5)$ , and  $\lambda_3 = 1.0395(4)$  where  $\lambda_1 < \lambda_2 < \lambda_3$ . Compared with other Heusler alloys [15,16,27,33,49,55,56], the sample with  $x = 0.3$  exhibits a smaller value of  $|1 - \lambda_2| = 1.7(5) \times 10^{-3}$ , which indicates a good geometric compatibility between the two phases. As a result, a small  $\Delta T_{\text{hys}}$  can be obtained, in agreement with the model prediction.

#### IV. CONCLUSIONS

In summary, we realized a very low thermal hysteresis of 2.3 K in the Ni-Mn-In-based Heusler alloys through a strategy of introducing V. Together with a strong magnetostructural coupling, the reversibility of magnetic-field-induced structural transition is improved for a low field change of 0–1 T in the composition  $\text{Ni}_{50.7}\text{Mn}_{33.4}\text{In}_{15.6}\text{V}_{0.3}$ . Thus, a highly reversible MCE could be fulfilled. By magnetic and caloric measurements, a considerable reversible  $\Delta S_m$  of

$5.1 \text{ J kg}^{-1} \text{ K}^{-1}$  is obtained at 278 K for a field change of 0–1 T field variation. In addition, a large reversible  $\Delta T_{ad}$  of  $-1.2 \text{ K}$  is achieved for this field change. On the basis of a crystallographic analysis, the transformation stretch tensor is calculated, which indicates a good geometric compatibility between the two phases in  $\text{Ni}_{50.7}\text{Mn}_{33.4}\text{In}_{15.6}\text{V}_{0.3}$ . This compatibility is found to be responsible for the small hysteresis. Our work provides a feasible method for the practical application of Ni-Mn-X-based Heusler alloys as magnetocaloric materials.

#### ACKNOWLEDGMENTS

The authors would like to thank A. J. E. Lefering, B. Zwart, and K. Goubitz for their technical help. This work was sponsored by NOW in the Domain Applied and Engineering Sciences (AES) Programme and the National Natural Science Foundation of China (Grants No. 51601092, No. 51571121, and No. 11604148). J. Liu gratefully acknowledges financial support from the China Scholarship Council.

- 
- [1] E. Brück, *J. Phys. D.* **38**, R381 (2005).
- [2] O. Gutfleisch, M. A. Willard, E. Brück, C. H. Chen, S. G. Sankar, and J. P. Liu, *Adv. Mater.* **23**, 821 (2011).
- [3] V. Franco, J. S. Blázquez, J. J. Ipus, J. Y. Law, L. M. Moreno-Ramírez, and A. Conde, *Prog. Mater. Sci.* **93**, 112 (2018).
- [4] V. K. Pecharsky and K. A. Gschneidner, Jr., *Phys. Rev. Lett.* **78**, 4494 (1997).
- [5] K. G. Sandeman, *Scr. Mater.* **67**, 566 (2012).
- [6] M. F. J. Boeije, P. Roy, F. Guillou, H. Yibole, X. F. Miao, L. Caron, D. Banerjee, N. H. van Dijk, R. A. de Groot, and E. Bruck, *Chem. Mater.* **28**, 4901 (2016).
- [7] O. Tegus, E. Brück, K. H. J. Buschow, and F. R. de Boer, *Nature (London)* **415**, 150 (2002).
- [8] F. Guillou, G. Porcari, H. Yibole, N. van Dijk, and E. Brück, *Adv. Mater.* **26**, 2671 (2014).
- [9] M. Maschek, X. You, M. F. J. Boeije, D. Chernyshov, N. H. van Dijk, and E. Brück, *Phys. Rev. B* **98**, 224413 (2018).
- [10] B. G. Shen, J. R. Sun, F. X. Hu, H. W. Zhang, and Z. H. Cheng, *Adv. Mater.* **21**, 4545 (2009).
- [11] Y. Y. Shao, J. Liu, M. Zhang, A. Yan, K. P. Skokov, D. Y. Karpenkov, and O. Gutfleisch, *Acta Mater.* **125**, 506 (2017).
- [12] T. Krenke, E. Duman, M. Acet, E. F. Wassermann, X. Moya, L. Mañosa, and A. Planes, *Nat. Mater.* **4**, 450 (2005).
- [13] X. Moya, L. Mañosa, A. Planes, S. Aksoy, M. Acet, E. F. Wassermann, and T. Krenke, *Phys. Rev. B* **75**, 184412 (2007).
- [14] M. Khana, N. Ali, and S. Stadler, *J. Appl. Phys.* **101**, 053919 (2007).
- [15] J. Liu, T. Gottschall, K. P. Skokov, J. D. Moore, and O. Gutfleisch, *Nat. Mater.* **11**, 620 (2012).
- [16] X. M. Sun, D. Y. Cong, Z. Li, Y. L. Zhang, Z. Chen, Y. Ren, K. D. Liss, Z. Y. Ma, R. G. Li, Y. H. Qu, Z. Yang, L. Wang, and Y. D. Wang, *Phys. Rev. Mater.* **3**, 034404 (2019).
- [17] L. Caron, N. T. Trung, and E. Brück, *Phys. Rev. B* **84**, 020414(R) (2011).
- [18] E. K. Liu, W. H. Wang, L. Feng, W. Zhu, G. J. Li, J. L. Chen, H. W. Zhang, G. H. Wu, C. B. Jiang, H. B. Xu, and F. de Boer, *Nat. Commun.* **3**, 873 (2012).
- [19] J. Liu, Y. Y. Gong, G. Z. Xu, G. Peng, I. A. Shah, N. ul Hassan, and F. Xu, *Sci. Rep.* **6**, 23386 (2016).
- [20] Y. Sutou, Y. Imano, N. Koeda, T. Omori, R. Kainuma, K. Ishida, and K. Oikawa, *Appl. Phys. Lett.* **85**, 4358 (2004).
- [21] T. Krenke, M. Acet, E. F. Wassermann, X. Moya, L. Mañosa, and A. Planes, *Phys. Rev. B* **72**, 014412 (2005).
- [22] T. Krenke, M. Acet, E. F. Wassermann, X. Moya, L. Mañosa, and A. Planes, *Phys. Rev. B* **73**, 174413 (2006).
- [23] R. Kainuma, Y. Imano, W. Ito, Y. Sutou, H. Morito, S. Okamoto, O. Kitakami, K. Oikawa, A. Fujita, T. Kanomata, and K. Ishida, *Nature (London)* **439**, 957 (2006).
- [24] T. Krenke, E. Duman, M. Acet, E. F. Wassermann, X. Moya, L. Mañosa, A. Planes, E. Suard, and B. Ouladdiaf, *Phys. Rev. B* **75**, 104414 (2007).
- [25] J. Liu, S. Aksoy, N. Scheerbaum, M. Acet, and O. Gutfleisch, *Appl. Phys. Lett.* **95**, 232515 (2009).
- [26] V. K. Sharma, M. K. Chattopadhyay, K. H. B. Shaeb, A. Chouhan, and S. B. Roy, *Appl. Phys. Lett.* **89**, 222509 (2006).
- [27] D. W. Zhao, J. Liu, X. Chen, W. Sun, Y. Li, M. X. Zhang, Y. Y. Shao, H. Zhang, and A. R. Yan, *Acta Mater.* **133**, 217 (2017).
- [28] T. Kihara, X. Xu, W. Ito, R. Kainuma, and M. Tokunaga, *Phys. Rev. B* **90**, 214409 (2014).
- [29] T. Gottschall, K. P. Skokov, D. Benke, M. E. Gruner, and O. Gutfleisch, *Phys. Rev. B* **93**, 184431 (2016).
- [30] T. Graf, C. Felser, and S. S. P. Parkin, *Prog. Solid State Chem.* **39**, 1 (2011).
- [31] T. Gottschall, K. P. Skokov, B. Frincu, and O. Gutfleisch, *Appl. Phys. Lett.* **106**, 021901 (2015).
- [32] T. Gottschall, E. Stern-Taulats, L. Mañosa, A. Planes, K. P. Skokov, and O. Gutfleisch, *Appl. Phys. Lett.* **110**, 223904 (2017).

- [33] Y. H. Qu, D. Y. Cong, X. M. Sun, Z. H. Nie, W. Y. Gui, R. G. Li, Y. Ren, and Y. D. Wang, *Acta Mater.* **134**, 236 (2017).
- [34] S. J. Kim, W. H. Ryu, H. S. Oh, and E. S. Park, *J. Appl. Phys.* **123**, 033903 (2018).
- [35] F. Scarpa, G. Tagliafico, and L. A. Tagliafico, *Renew. Sust. Energ. Rev.* **50**, 497 (2015).
- [36] R. Bjørk, A. Smith, C. Bahl, and N. Pryds, *Int. J. Refrig.* **34**, 1805 (2011).
- [37] B. Monfared, R. Furberg, and B. Palm, *Int. J. Refrig.* **42**, 69 (2014).
- [38] G. Porcari, F. Cugini, S. Fabbri, C. Pernechele, F. Albertini, M. Buzzi, M. Mangia, and M. Solzi, *Phys. Rev. B* **86**, 104432 (2012).
- [39] T. Roisnel and J. Rodríguez-Carvajal, *Mater. Sci. Forum.* **378-381**, 118 (2001).
- [40] S. Singh, L. Caron, S. W. D'Souza, T. Fichtner, G. Porcari, S. Fabbri, C. Shekhar, S. Chadov, M. Solzi, and C. Felser, *Adv. Mater.* **28**, 3321 (2016).
- [41] A. Planes, T. Castán, and A. Saxena, *Phil. Trans. R. Soc. A* **374**, 20150304 (2016).
- [42] B. M. Wang, Y. Liu, L. Wang, S. L. Huang, Y. Zhao, Y. Yang, and H. Zhang, *J. Appl. Phys.* **104**, 043916 (2008).
- [43] S. Aksoy, T. Krenke, M. Acet, and E. F. Wassermann, *Appl. Phys. Lett.* **91**, 241916 (2007).
- [44] T. Gottschall, K. P. Skokov, R. Burriel, and O. Gutfleisch, *Acta Mater.* **107**, 1 (2016).
- [45] L. Caron, Z. Q. Ou, T. T. Nguyen, D. T. Cam Thanh, O. Tegus, and E. Brück, *J. Magn. Magn. Mater.* **321**, 3559 (2009).
- [46] B. Kaeswurm, V. Franco, K. P. Skokov, and O. Gutfleisch, *J. Magn. Magn. Mater.* **406**, 259 (2016).
- [47] M. Fries, L. Pfeuffer, E. Bruder, T. Gottschall, S. Ener, L. V. B. Diop, T. Grob, K. P. Skokov, and O. Gutfleisch, *Acta Mater.* **132**, 222 (2017).
- [48] See Supplemental Material at <http://link.aps.org/supplemental/10.1103/PhysRevMaterials.3.084409>. Figure S1 shows the magnetic entropy change  $\Delta S_m$  under field change of 0–5 T for sample with  $x = 0.3$  by the Maxwell relation and the transformed mass fraction method on the basis of isothermal  $M$ - $B$  curves. Figure S2 shows the reversible value of  $\Delta S_m$  under field change of 0–5 T for sample with  $x = 0.3$  calculated by the transformed mass fraction method.
- [49] Y. H. Qu, D. Y. Cong, S. H. Li, W. Y. Gui, Z. H. Nie, M. H. Zhang, Y. Ren, and Y. D. Wang, *Acta Mater.* **151**, 41 (2018).
- [50] J. Cui J, Y. S. Chu, O. Famodu, Y. Furuya, J. Hattrick-Simpers, R. D. James, A. Ludwig, S. Thienhuas, M. Wutting, Z. Zhang, and I. Takechi, *Nat. Mater.* **5**, 286 (2006).
- [51] Y. Song, X. Chen, V. Dabade, T. W. Shield, and R. D. James, *Nature (London)* **502**, 85 (2013).
- [52] X. Chen, Y. Song, N. Tamura, and R. D. James, *J. Mech. Phys. Solids* **93**, 34 (2016).
- [53] C. Chluba, W. Ge, R. L. de Miranda, J. Strobel, L. Kienle, E. Quandt, and M. Wuttig, *Science* **348**, 1004 (2015).
- [54] P. Devi, M. G. Zavareh, C. S. Mejía, K. Hofmann, B. Albert, C. Felser, M. Nicklas, and S. Singh, *Phys. Rev. Mater.* **2**, 122401(R) (2018).
- [55] V. Srivastava, X. Chen, and R. D. James, *Appl. Phys. Lett.* **97**, 014101 (2010).
- [56] K. P. Bhatti, S. El-Khatib, V. Srivastava, R. D. James, and C. Leighton, *Phys. Rev. B* **85**, 134450 (2012).
- [57] K. F. Hane and T. W. Shield, *Acta Mater.* **47**, 2603 (1999).
- [58] H. Yan, Y. Zhang, N. Xu, A. Senyshyn, H. Brokmeier, C. Esling, X. Zhao, and L. Zuo, *Acta Mater.* **88**, 375 (2015).
- [59] S. Singh, P. Kushwaha, F. Scheibel, H. P. Liermann, S. R. Barman, M. Acet, C. Felser, and D. Pandey, *Phys. Rev. B* **92**, 020105(R) (2015).